Supporting information

Extraordinary dual-ion electrochemical deionization capacity and energy efficiency enabled by coupling of $Na_3Fe_2(PO_4)_3$ and NiVAl layered double hydroxides electrodes

Pei Zhang[1], Lei Yao[2], Xiangzhong Ren[1], Yongliang Li[1], and Libo Deng*[1]

[1]College of Chemistry and Environmental Engineering, Shenzhen University, Shenzhen 518060, China

[2]Shenzhen Key Laboratory of Special Functional Materials, Shenzhen Engineering Laboratory for Advanced Technology of Ceramics, Guangdong Research Center for Interfacial Engineering of Functional Materials, College of Materials Science and Engineering, Shenzhen University, Shenzhen 518060, P. R. China

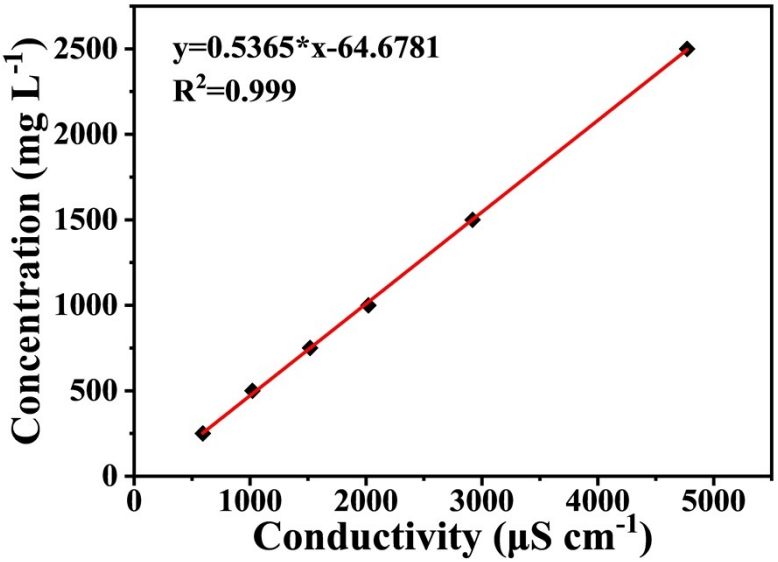

Fig. S1 The relationship between the conductivity and concentration of NaCl solution.

* Corresponding author: Denglb@szu.edu.cn; Tel: +86-755-26536157

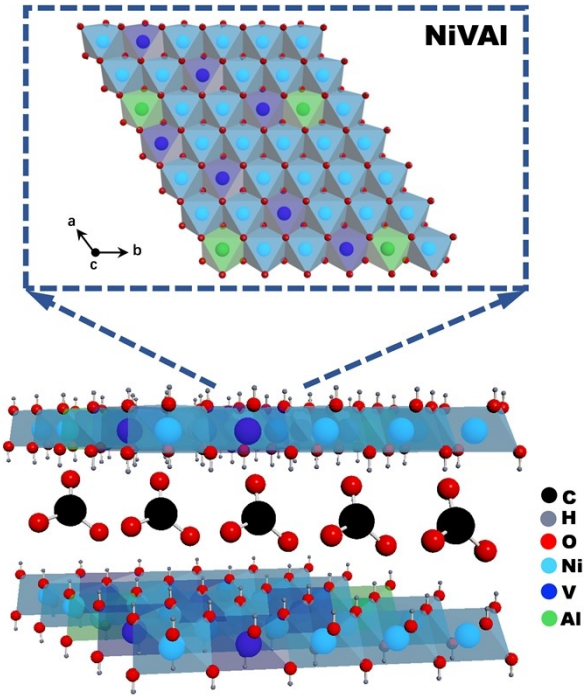

Fig. S2 Top-view and front view schematic diagram of NiVAl-LDH crystal with Cl^- in the interlayer.

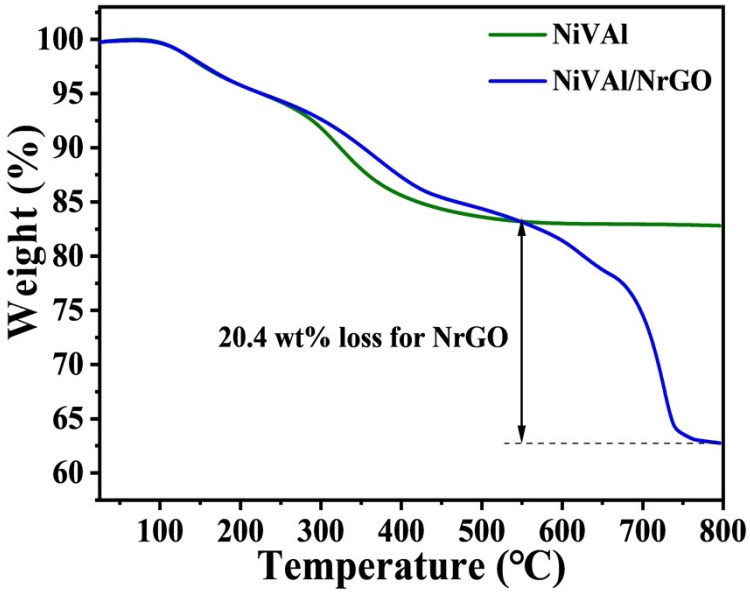

Fig. S3 TGA curves of NiVAl and NiVAl/NrGO.

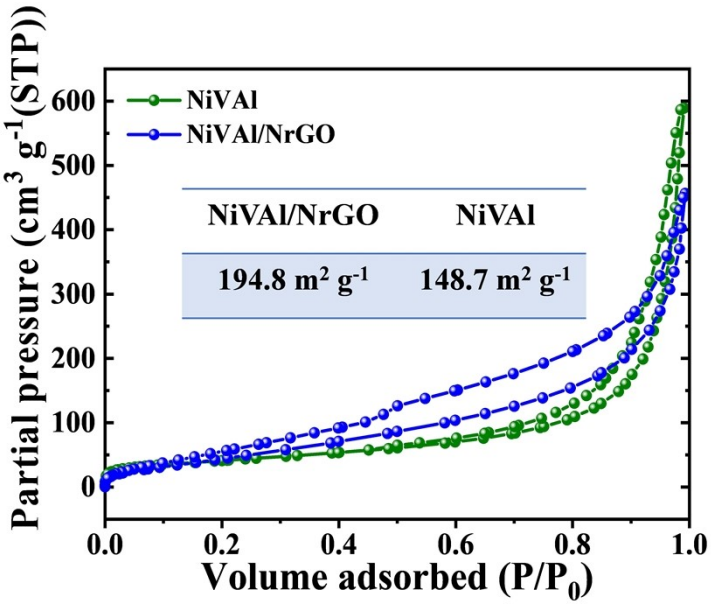

Fig. S4 N_2 adsorption–desorption isotherms and BET analysis of NiVAl and NiVAl/NrGO.

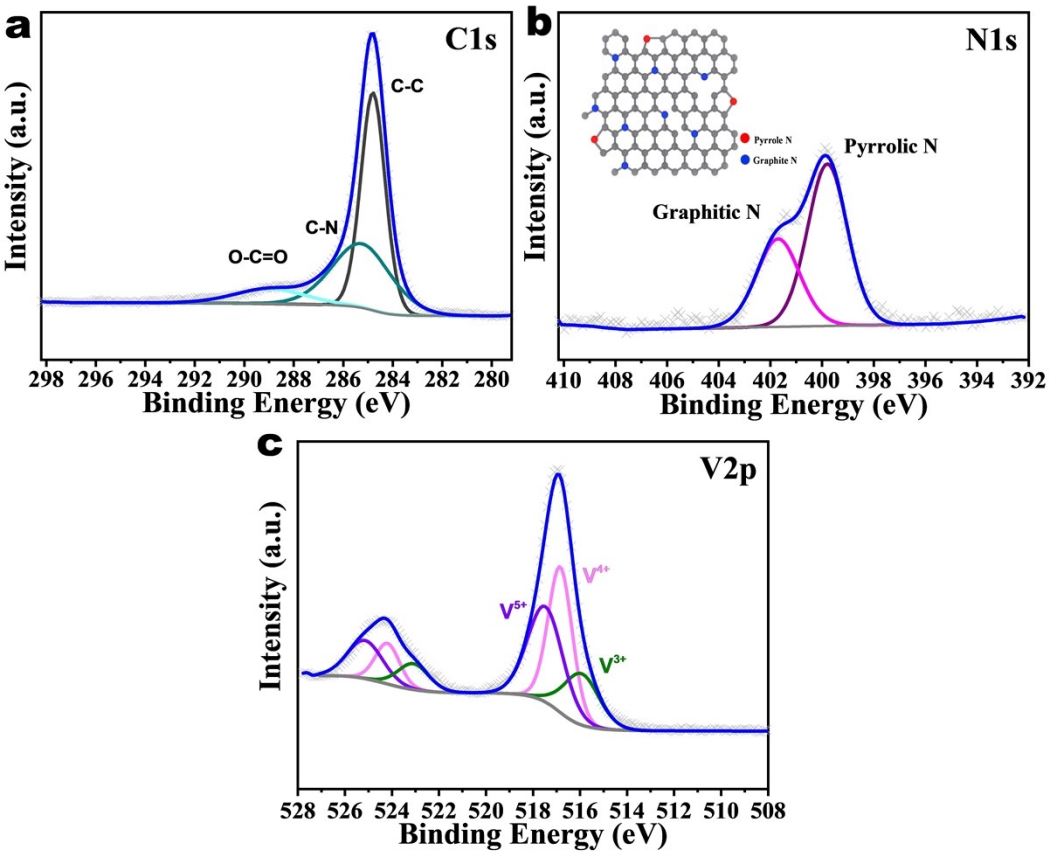

Fig. S5 High-resolution XPS spectra of: (a) C1s; (b) N1s; and (c) V2p in NiVAl/NrGO.

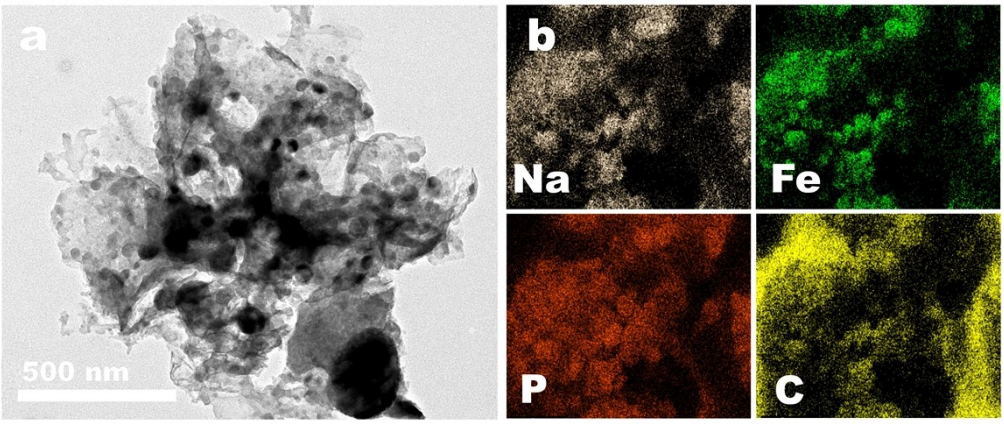

Fig. S6 (a) TEM image of NFP@C and (b) EDS elemental mapping.

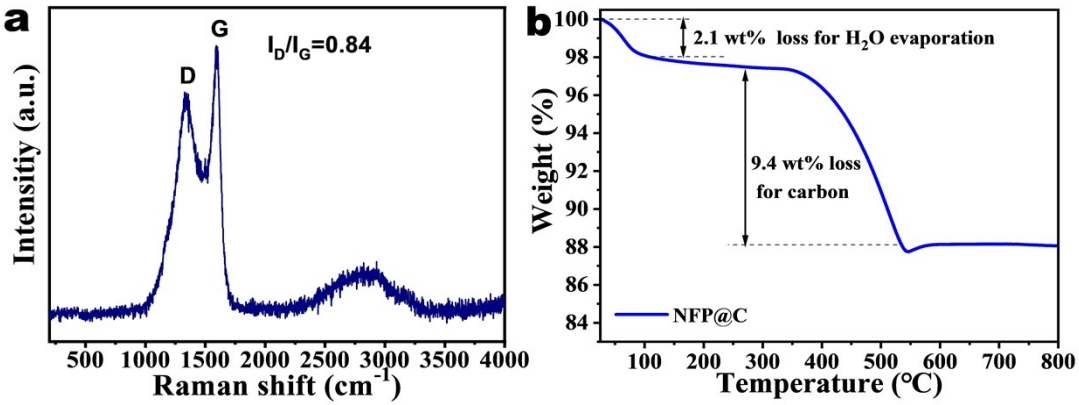

Fig. S7 (a) Raman spectrum and (b) TGA curve of NFP@C.

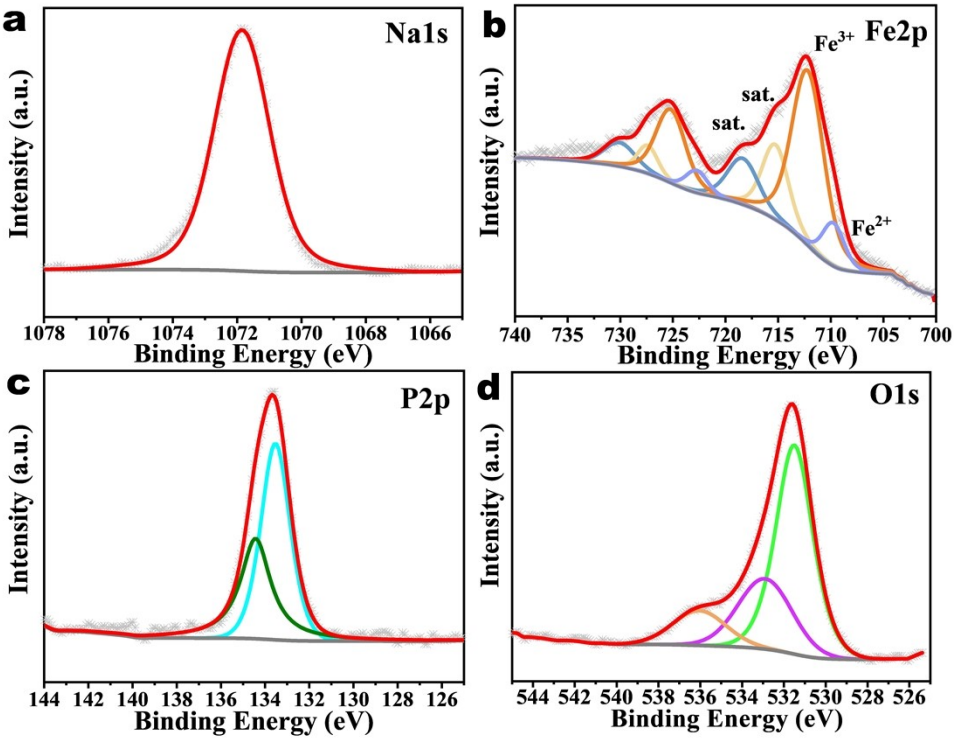

Fig. S8 XPS high-resolution spectra of the as-prepared NFP@C nanocomposite: (a) Na1s; (b) Fe2p; (c) P2p; and (d) O1s.

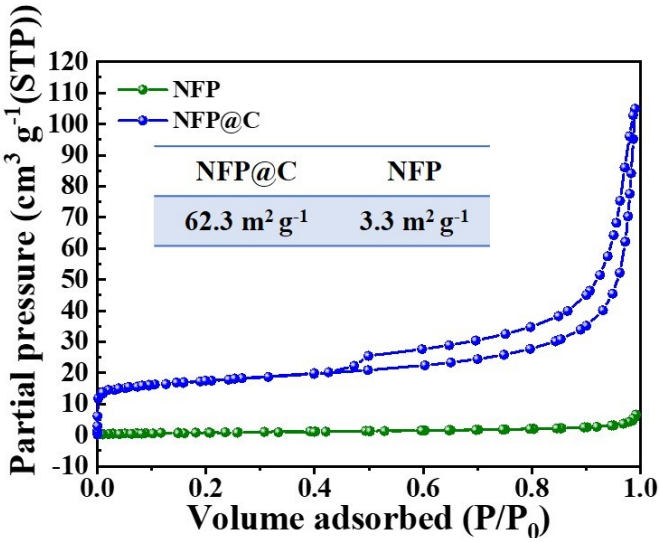

Fig. S9 N_2 adsorption–desorption isotherms and specific surface analysis of NFP@C and NFP.

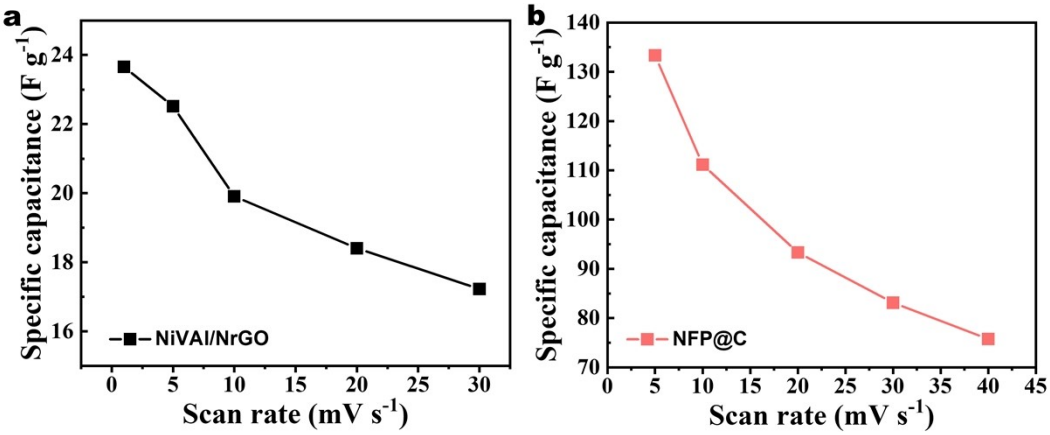

Fig. S10 Specific capacitances of: (a) NiVAl/NrGO and (b) NFP@C at different scan rates determined using a CV method.

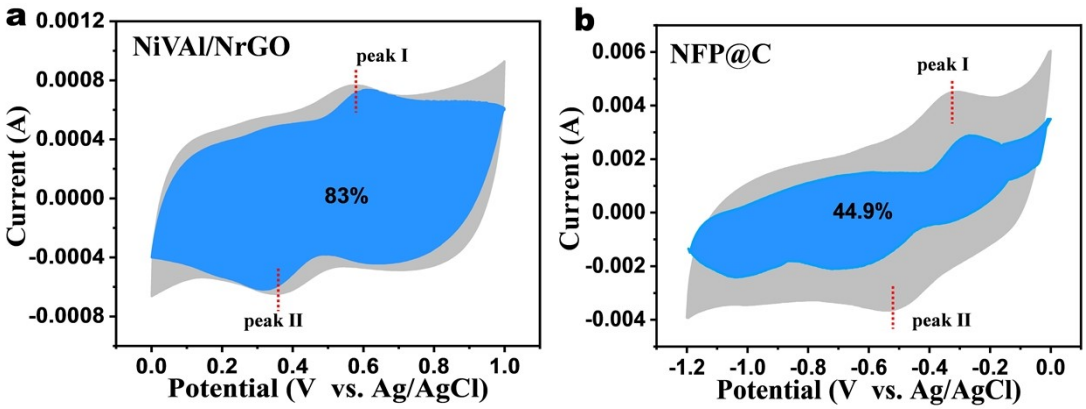

Fig. S11 CV curves showing the capacitive (blue area) and diffusion-controlled (grey area) contributions to intercalation process for: (a) NiVAl/NrGO and (b) NFP@C at a scan rate of 20 mV s^{-1}.

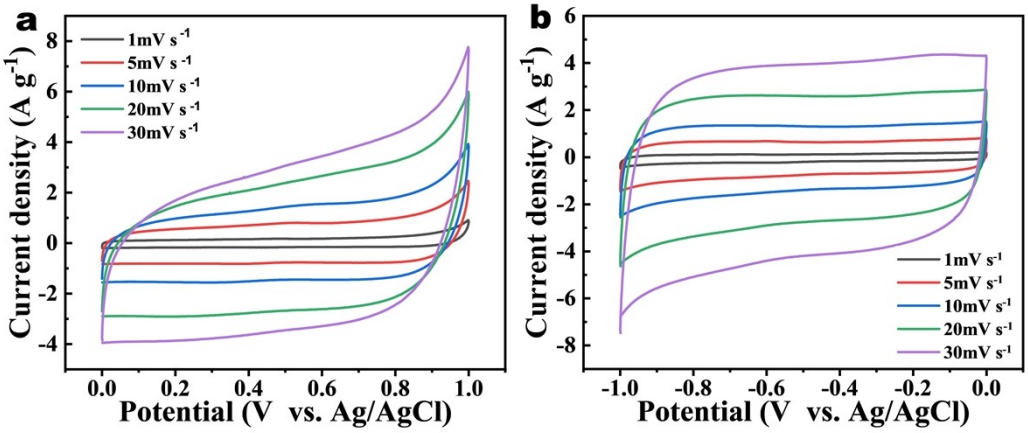

Fig. S12 CV curves of AC in different potential ranges. Electrolyte: 1 M NaCl.

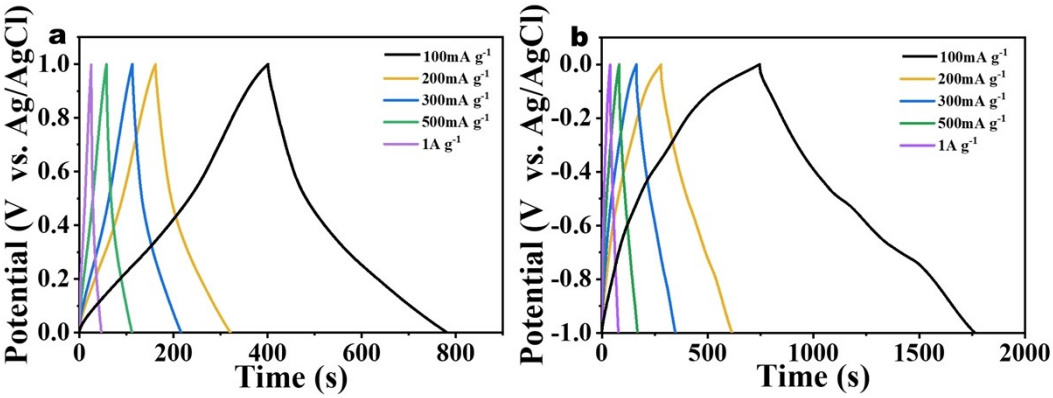

Fig. S13 GCD curves acquired in a three-electrode cell for: (a) NiVAl/NrGO and (b) NFP@C at different current densities. Electrolyte: 1 M NaCl.

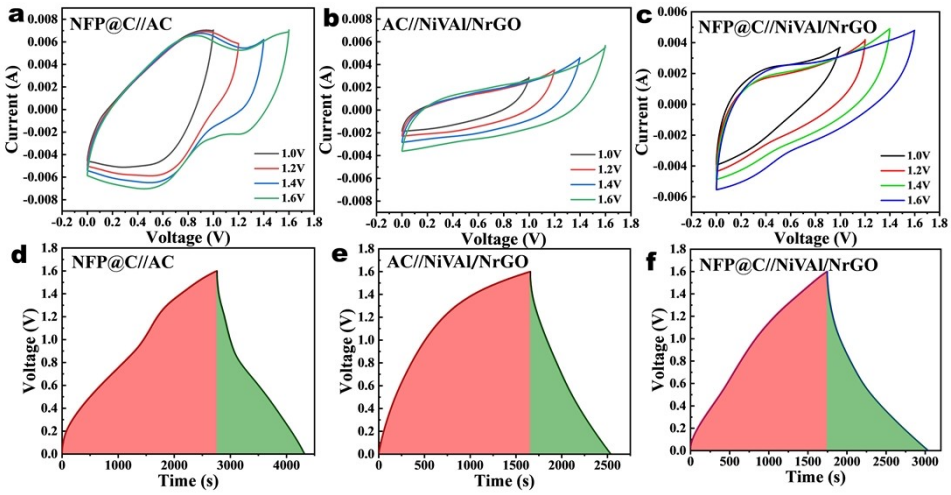

Fig. S14 (a-c) CV curves (5mV s^{-1}) acquired in different voltage ranges for the three EDI systems and (d-f) GCD curves measured at a current density of 50 mA g^{-1}. The red and green shaded areas indicate the energy consumed and recoverable during charge and discharge. Electrolyte: 1000 mg L^{-1} NaCl.

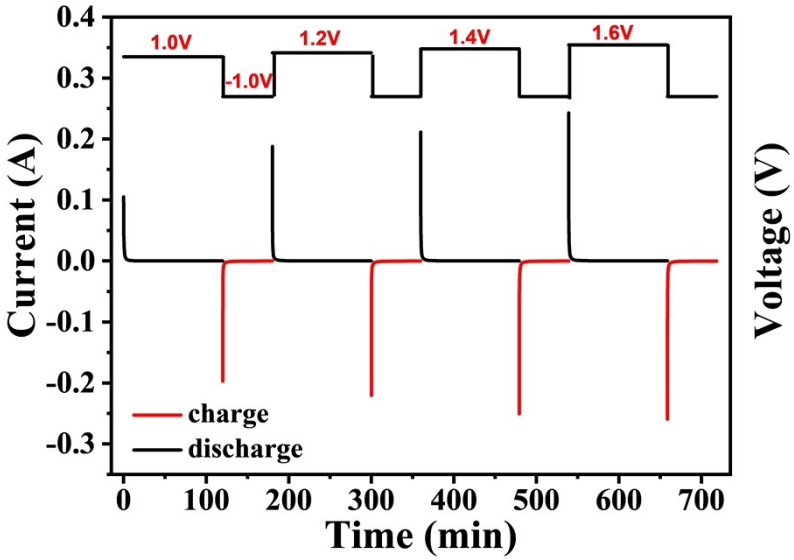

Fig. S15 Chronocoulometry curves of the DEDI system tested at different charging voltages. Electrolyte: 1000 mg L^{-1} NaCl.

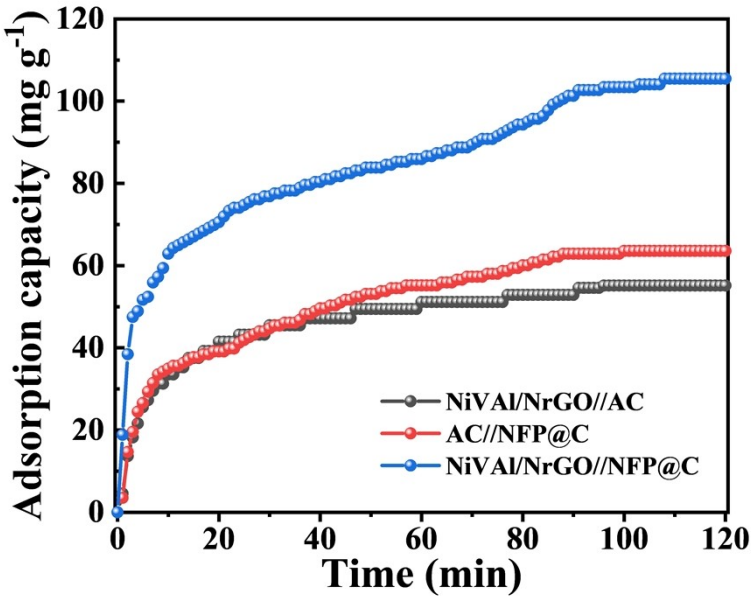

Fig. S16 Comparison of salt adsorption capacity of AC//NFP@C, NiVAl/NrGO//AC and NiVAl/NrGO//NFP@C systems. Electrolyte: 1000 mg L^{-1} NaCl.

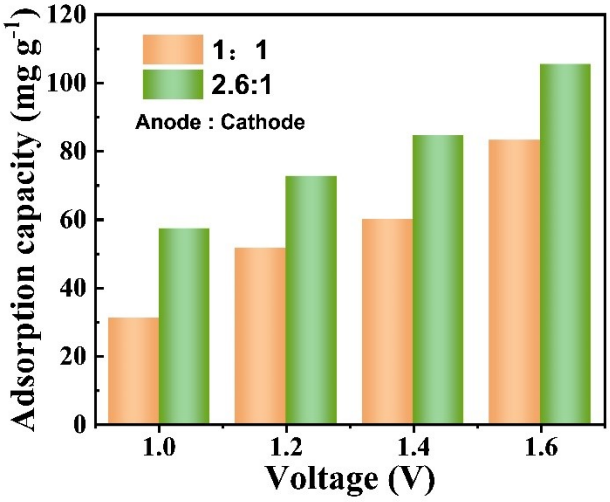

Fig. S17 Comparison of desalination performance of NiVAl/NrGO//NFP@C system constructed with different mass ratios.

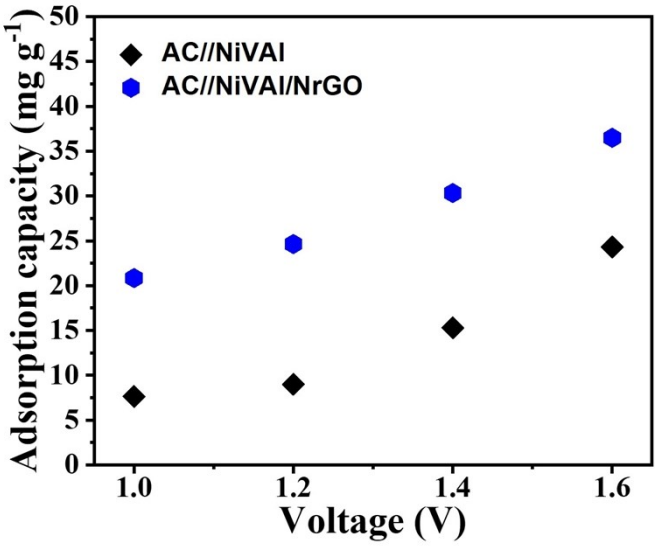

Fig. S18 Comparison of salt adsorption capacity for NiVAl//AC and NiVAl/NrGO//AC. Concentration of the salt: 250 mg L^{-1}.

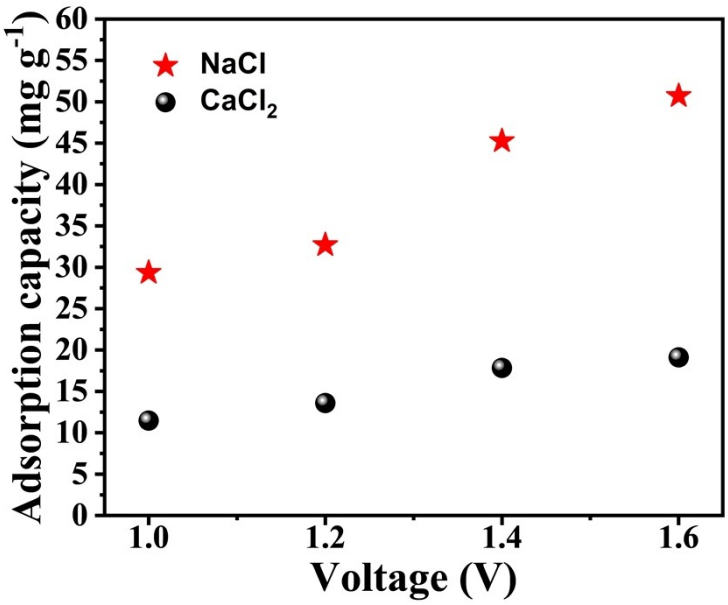

Fig. S19 Comparison of the adsorption capacity towards NaCl and $CaCl_2$ by the AC//NFP@C system. Concentration of the salts: 500 mg L^{-1}.

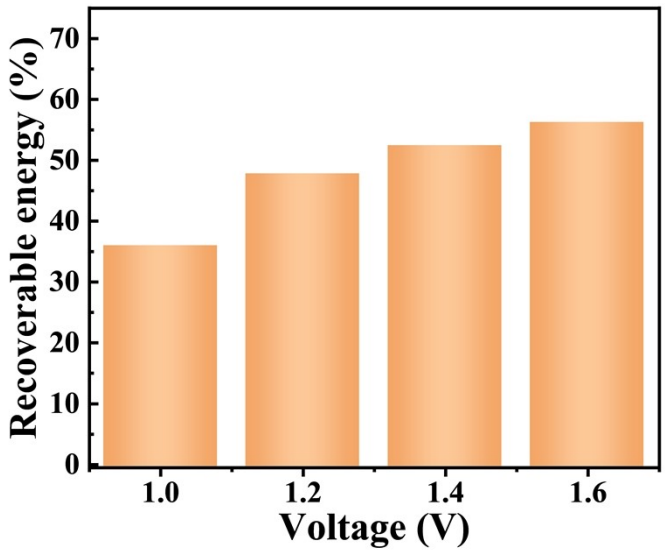

Fig. S20 The fraction of recoverable energy among the energy consumed for NiVAl/NrGO//NFP@C at various voltages. Electrolyte: 1000 mg L^{-1} NaCl.

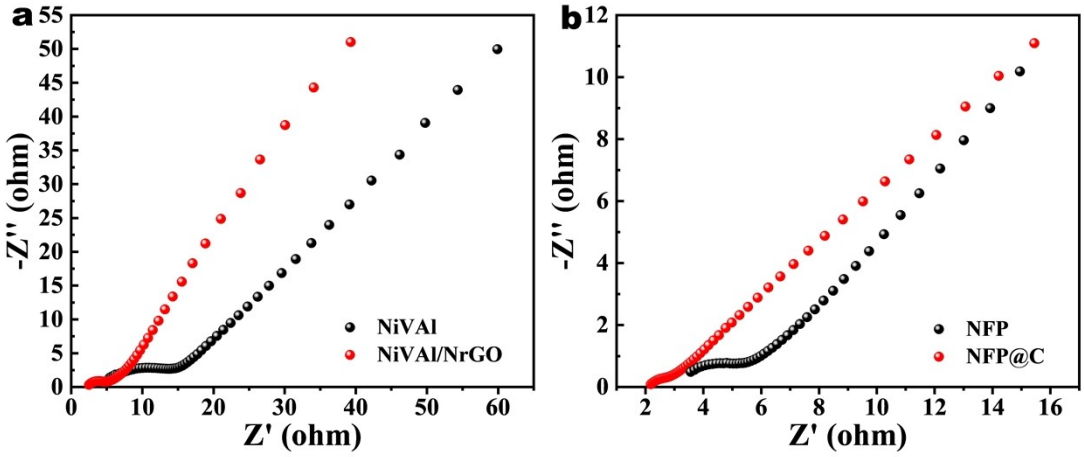

Fig. S21 Nyquist plots of the NiVAl, NiVAl/NrGO, NFP and NFP@C electrodes tested in a three-electrode system. Electrolyte: 1 M NaCl.

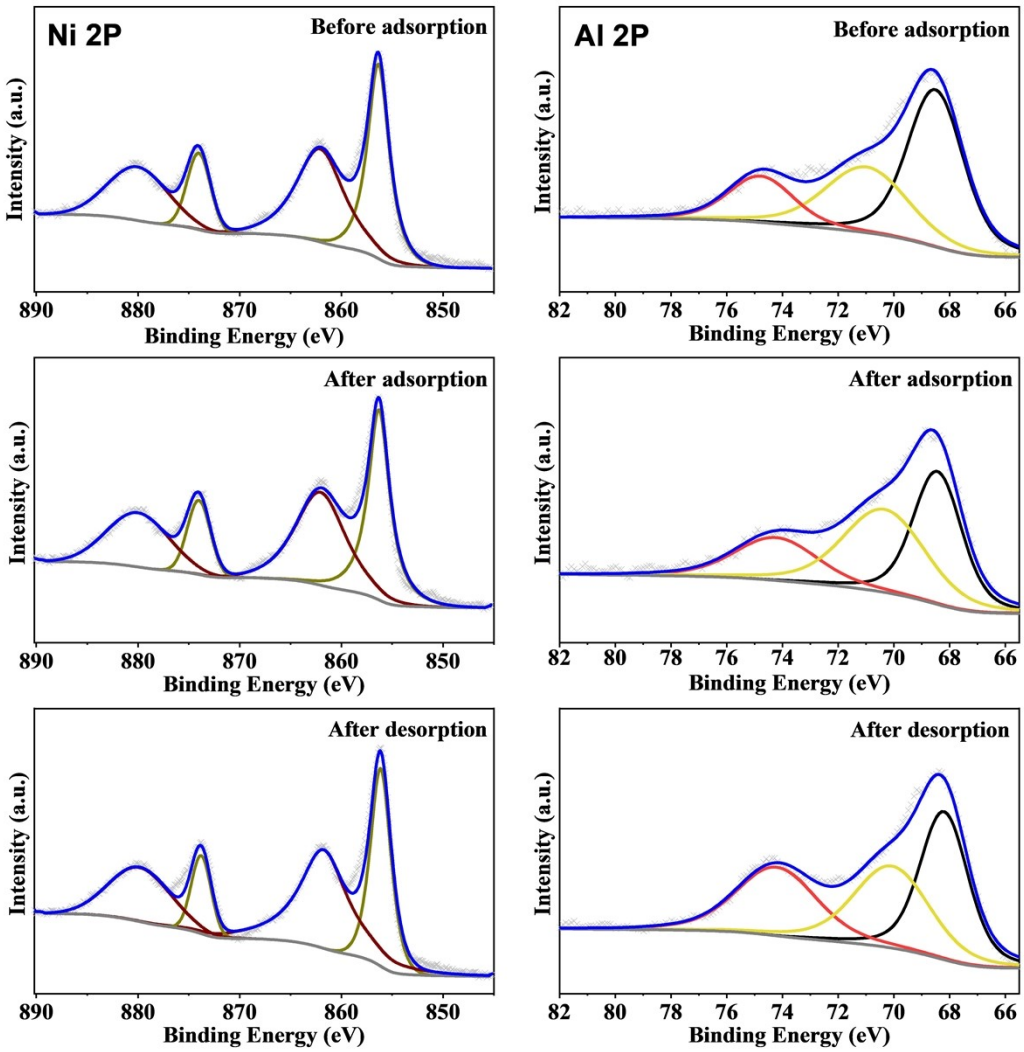

Fig. S22 XPS spectra of Ni2P and Al2P of NiVAl /NrGO at different states.

Table S1. Comparison between NFP@C//NiVAl/NrGO and other CDI applications.

Cathode	Anode	Voltage (V)	NaCl Concentration (mg L^{-1})	Desalination capacity (mg g^{-1})	Ref.
VO_xNT_s/CNPT	AC	1.6	350.6	25	1
$Na_2FeP_2O_7$	AC	1.2	5844	30.2	2
MoS_2/NOMC	AC	1.6	250	28.82	3
G-V_2O_5	G-V_2O_5	1.2	584	12.5	4
NaOH-$Ti_3C_2T_x$	AC	1.2	500	16.02	5
NaxCoO_2	AC	1.4	500	92.9	6
FeHCF@3DNC	AC	1.2	5844	60.5	7
TiO_2@COF-$_2$	AC	1.6	200	33.66	8
$Na_3MnTi(PO_4)_3$/C	AC	1.2	2000	72.2	9
Ti_3C_2 MXene	AC	1.2	500	26.8	10
MnO_2	Ppy/AC	1.4	820	52.9	11
PVDF	CS +3GA	1.2	1000	16.7	12
$Na_{1.1}V_3O_{7.9}$@rGO	Ag@rGO	1.4	2000	82.2	13
CLF@$Ti_3C_2T_x$	CLF@$Ti_3C_2T_x$	1.2	600	34	14
NFP@C	NiVAl /NrGO	1.6	1000	105.5	this work

Supplementary references

1. D.M. Sayed, M.S. El-Deab, N.K. Allam, Multi-walled vanadium oxide nanotubes modified 3D microporous bioderived carbon as novel electrodes for hybrid capacitive deionization, Sep. Purif. Technol. 2021, 266, 118597.
2. S. Kim, J. Lee, C. Kim, J. Yoon, $Na_2FeP_2O_7$ as a Novel material for hybrid capacitive deionization, Electrochim. Acta. 2016, 203, 265-271.
3. S. Tian, X. Zhang, Z. Zhang, Novel MoS_2/NOMC electrodes with enhanced capacitive deionization performances, Chem. Eng. J. 2021, 409, 128200.
4. A. Baburaj, A.B. Puthirath, A. Jain, D. Palanisamy, D. Salpekar, J. Balachandran, M.A. Kabbani, F.C.R. Hernandez, G. Hughes, G. Babu, P.M. Ajayan, Multilayer graphene coated vanadium(V) oxide as electrodes for intercalation based brackish water desalination, 2D Mater. 2020, 7, 45025.
5. B. Chen, A. Feng, R. Deng, K. Liu, Y. Yu, L. Song, MXene as a cation-selective cathode material for asymmetric capacitive deionization, ACS Appl. Mater. Inter. 2020, 12, 13750-13758.
6. R. Zhou, J. Li, W. Wei, X. Li, M. Luo, Atomic substituents effect on boosting desalination performances of Zn-doped Na_xCoO_2, Desalination 2020, 496, 114695.
7. A. Gong, Y. Zhao, M. He, B. Liang, K. Li, High-performance desalination of three-dimensional nitrogen-doped carbon framework reinforced Prussian blue in capacitive deionization, Desalination 2021, 505, 114997.
8. X. Liu, S. Zhang, G. Feng, Z. Wu, D. Wang, M.D. Albaqami, B. Zhong, Y. Chen, X. Guo, X. Xu, Y. Yamauchi, Core−shell MOF@COF motif hybridization: selectively functionalized precursors for titanium dioxide nanoparticle-embedded nitrogen-rich carbon architectures with superior capacitive deionization performance, Chem. Mater. 2021, 33, 1657-1666.
9. S. Wang, G. Wang, C. He, N. Gao, B. Lu, L. Zhao, J. Weng, S. Zeng, C. Li, Enabling superior hybrid capacitive deionization performance in NASICON-structured $Na_3MnTi(PO_4)_3$/C by incorporating a two-species redox reaction, J. Mater. Chem. A 2021, 9, 6898-6904.
10. L. Guo, X. Wang, Z.Y. Leong, R. Mo, L. Sun, H.Y. Yang, Ar plasma modification of 2D MXene $Ti_3C_2T_x$ nanosheets for efficient capacitive desalination, FlatChem. 2018, 8, 17-24.
11. G. Tan, S. Lu, N. Xu, D. Gao, X. Zhu, Pseudocapacitive behaviors of polypyrrole grafted activated carbon and MnO_2 electrodes to enable fast and efficient membrane-free capacitive deionization,

Environ. Sci. Technol. 2020, 54, 5843-5852.

12. J. Weng, S. Wang, G. Wang, P. Zhang, B. Lu, H. Wang, J. Jiang, C. Li, Carbon electrode with cross-linked and charged chitosan binder for enhanced capacitive deionization performance, Desalination, 2021, 505, 114979.
13. Z. Yue, Y. Ma, J. Zhang, H. Li, Pseudo-capacitive behavior induced dual-ion hybrid deionization system based on Ag@rGO ‖ $Na_{1.1}V_3O_{7.9}$@rGO, J. Mater. Chem. A 2019, 7, 16892-16901.
14. S. Anwer, D.H. Anjum, S. Luo, Y. Abbas, B. Li, S. Iqbal, K. Liao, 2D $Ti_3C_2T_x$ MXene nanosheets coated cellulose fibers based 3D nanostructures for efficient water desalination, Chem. Eng. J. 2021, 406, 126827.